Appl. Phys. B (2016) 122:155
DOI 10.1007/s00340-016-6412-1

Applied Physics B
Lasers and Optics

Plasmonic electric near-field enhancement in self-organized gold nanoparticles in macroscopic arrays

V. Mondes[1] · E. Antonsson[1] · J. Plenge[1] · C. Raschpichler[1] · I. Halfpap[1] · A. Menski[1] · C. Graf[1] · M. F. Kling[2] · E. Rühl[1]

Received: 2 August 2015 / Accepted: 11 April 2016
© Springer-Verlag Berlin Heidelberg 2016

Abstract When plasmonic nanoparticles are incorporated into nanostructures and they are exposed to external optical fields, plasmonic coupling causes electric near-field enhancement which is significantly larger than that of isolated nanoparticles. We report on the plasmonic coupling in arrays of gold nanospheres (20 ± 3 and 50 ± 4 nm) prepared by colloidal chemistry and self-organization. This yields field enhancement in arrays with areas of several mm^2 and provides an alternative approach to lithographic methods for preparation of nanostructures for plasmonic applications. Gold nanospheres are surface-functionalized by organic ligands, which define the interparticle distance in the array upon self-organization of the nanoparticles. The experiments are accompanied by finite-difference time-domain simulations, which quantify the dependence of the field enhancement on the interparticle distance.

1 Introduction

Electromagnetic fields of suitable frequency can induce the collective oscillation of the conduction band electrons in materials, which is known to be due to the excitation of surface plasmons [1]. For metal nanoparticles, the localized surface plasmons appear near the nanoparticle surface and their properties strongly depend on the size and shape of the nanoparticles as well as on the local environment [2]. Metallic nanoparticles that are arranged in close-packed structures show high-amplitude localized electromagnetic fields, which are due to the coupling between neighboring nanoparticles [1–3].

Recently, there has been increased interest in plasmonic nanostructures due to their promising applications [4]. Unique possibilities to guide and localize radiation by nanoscale structures lead to various applications, such as in surface-enhanced Raman scattering [5–10], photovoltaics [11], and imaging and microscopy techniques, e.g., medical diagnostics [12]. For imaging, the detected radiation can come from a range of nonlinear photon emission channels including white-light supercontinuum generation [13] and second [14, 15], third [16], and fifth [17] harmonic generation.

Ordered metallic nanostructures on the nanometer scale are generally prepared using either of two preparation schemes: (1) lithographic methods, in which, e.g., photon, electron, or ion beams are used to prepare ordered nanostructures starting from solid films [3, 15, 18, 19] or (2) using modern methods of colloidal chemistry [20], where the nanoparticles are formed from readily available stock chemicals and the nanostructuring is achieved using self-organization [10, 21]. In addition to these general schemes, combinations of both approaches have been reported, such as the formation of ordered nanostructures by using periodic arrays of colloidal nanoparticles as masks for lithography [22, 23] or by combining colloidal self-assembly with microcontact printing techniques [24].

Lithographic methods yield well-defined nanoscopic systems of various morphologies, size, and chemical composition. However, the devices used for lithography are complex and expensive [25–30], and the preparation

This article is part of the topical collection "Ultrafast Nanooptics" guest edited by Martin Aeschlimann and Walter Pfeiffer.

✉ E. Rühl
ruehl@zedat.fu-berlin.de

[1] Physical Chemistry, Freie Universität Berlin, Takustr. 3, 14195 Berlin, Germany

[2] Physics Department, Ludwig-Maximilians-Universität, Am Coulombwall 1, 85748 Garching, Germany

Published online: 17 May 2016

of samples sizes of the order of several mm^2 can be challenging [3, 19, 25–28]. Preparation of nanostructures from colloidal chemistry and self-organization appears to be a straightforward way to prepare inexpensive nanostructures of well-defined morphology where the arrays can exhibit large areas reaching into the square centimeter regime. However, the preparation of highly ordered nanostructures of large size may also be challenging [10]. This is the major motivation for the present work.

Modern methods of colloidal chemistry yield metallic and metal-dielectric nanoparticles in narrow size distribution [31–37]. These colloids are synthesized with well-defined and controllable internal structure, shape, chemical composition, and surface functionalization. This also allows for tailoring the optical properties of the nanoscopic objects according to their specific use [38–46]. Examples of the various nanoparticle architectures that have been reported before include metal particles with silica shells [39, 40], dielectric cores with metallic shells [47], rods [43, 44], cubes [48, 49], prisms [50], and cages [51]. Self-organization of such nanometer to micrometer particles yields highly ordered two- or three-dimensional structures. These are required for plasmonic applications, where metallic nanoparticles are used. Ordered arrays of nanoparticles prepared by colloidal chemistry have been prepared and characterized before [52, 53]. It was shown that this approach offers also a convenient way to tune the nanoparticle properties, such as their shape [54, 55] and chemical composition [56, 57].

Kim et al. [18] reported on the generation of XUV radiation in gaseous argon when the gas is in the vicinity of plasmonic bow-tie structures. The intensity of the laser radiation was orders of magnitude lower than the intensity generally needed for high harmonic generation in a gaseous sample, so that a femtosecond oscillator was sufficient for generating XUV radiation. This was interpreted as an indication for the process being initiated through locally enhanced electric fields at the corners of bow-tie structures. The plasmonic coupling between these structures increases the local electric field amplitude to intensities that are sufficiently high for XUV generation. Reproduction of the plasmon-enhanced high harmonic generation reported by Kim et al. has been proven to be difficult [58], and an alternative interpretation of the measured XUV photon emission has been proposed [17, 59]. Distinct lines in the emission spectrum evidently do not stem from the coherent process of high harmonic generation rather than from field-enhanced atomic line emission due to relaxation of excited neutral and ionic argon atoms in the gas. Despite this, the principle of coherent XUV light generation in rare gases due to plasmonically enhanced near fields in nanostructures was recently studied theoretically by Yang et al. [60], where simulations employing the finite element method indicate that self-organized spherical Au nanoparticles give rise to greatly enhanced near fields. These are in principle sufficient for the formation of harmonics radiation. In the present work, experimental evidence for electric near-field enhancement is presented, which supports the theoretical predictions of Yang et al. [60] that arrays of self-organized Au particles represent a feasible way to achieve locally enhanced electric near-field amplitudes due to nanoplasmonic coupling.

2 Experimental method

The experimental setup is schematically shown in Fig. 1. A Ti:sapphire oscillator (Vitesse-800, Coherent) is used to generate radiation pulses with a central wavelength of 800 nm and a pulse length of 85 ± 5 fs. The photon bandwidth is 11 nm (full width at half maximum) at a repetition rate of 80 MHz [61, 62].

An 8-mm-focal length lens is used to focus the femtosecond laser pulses onto the ordered Au nanoparticles, which are arranged as a thin film on a sapphire substrate. The peak intensity in the laser focus is estimated to be 10^8 W/cm^2, which is below the damage threshold of the nanoparticles [63]. The photon emission from the ordered gold nanoparticles is parallelized using a lens and is subsequently focused onto a multicore fiber after removal of the scattered 800-nm radiation using a band-pass filter. The analysis of the spectral distribution of the photon emission is performed by using a fluorescence spectrometer (iHr 550, Jobin-Yvon), where the photon emission is dispersed using a 300 lines/mm grating and the monochromatized radiation is detected by a charge-coupled device (CCD)

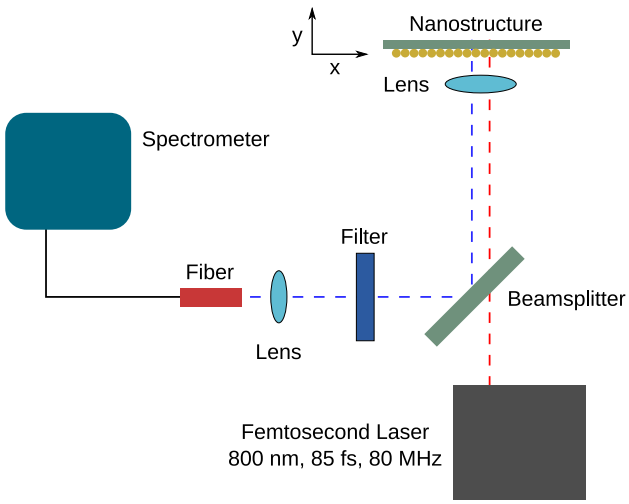

Fig. 1 Schematic view of the experimental setup for detecting spatially resolved photon emission from ordered nanoparticles excited by femtosecond laser pulses. See text for details

camera (Symphony, Jobin-Yvon). Spatially resolved photon emission is detected by placing the sample on a movable support in the plane that is perpendicular to the laser propagation direction. This is accomplished by using a translation stage.

The shape of the nanoparticles is an important parameter for plasmonic applications. Therefore, citrate-functionalized spherical gold nanoparticles with a diameter of 50 ± 4 nm are purchased from British BioCell International. The shape and size distribution are determined by electron microscopy.

The formation of smaller nanoparticles with diameters in the range of 10–20 nm is realized by sodium citrate reduction [64]. Ultrapure water and 1 % $HAuCl_4$ aqueous solution are stirred and heated in a glass flask. When the solution boils, 1 % sodium trihydrate solution is quickly added, which turns the initially colorless solution swiftly red. The mixture is heated for 10 min to ensure complete nanoparticle formation and is then placed to cool over night.

The spherical nanoparticles are arranged into arrays on a sapphire substrate by colloidal self-assembly at a water–toluene interface [21]. Gold nanoparticles dispersed in water are covered by a layer of toluene. Ethanol is added until the gold nanoparticles are captured on the water–toluene interface. The toluene is then removed by a syringe until the gold nanoparticles captured on the interface form a close-packed monolayer. A sapphire substrate is immersed into the mixture at an angle of 5°–10°, and the nanoparticle monolayer film is attached to the substrate by lifting it out of the mixture. This yields a close-packed monolayer of nanoparticles on the substrate. The ordering of the nanoparticles in the arrays is characterized by scanning electron microscopy (Hitachi SU-8030). The electron beam is typically accelerated by 5 kV, yielding a typical spatial resolution of 1.5 nm.

A commercial simulation software is used to perform the simulations [FDTD Solutions V8, Lumerical Inc., Vancouver (Canada)] using the finite-difference time-domain method, which solves the time-dependent Maxwell equations on a discrete mesh [65].

3 Results and discussion

The spectral characterization of photon emission from an ordered array of gold nanospheres is shown in Fig. 2.

This signal is due to nonlinear optical processes when the nanospheres are irradiated by weak femtosecond laser pulses at a central wavelength of 800 nm. The Au nanospheres have a diameter of 20 ± 3 nm and are surface functionalized by citrate ligands. An electron micrograph of a section of the investigated array of nanospheres is shown in Fig. 2c, which indicates that the particles are mostly close packed and some defects are observed. It cannot be entirely ruled out that no multilayers occur at all within the square centimeter area of the arrays. However, electron microscopy clearly reveals that monolayers dominate. Figure 2a shows the spectral regime corresponding to the third harmonic of the fundamental frequency, which is found at 267 nm, indicating that the local electric field at the surface of the Au nanospheres is sufficiently high to support this nonlinear photon conversion process. In Fig. 2b, the spectral regime containing the second harmonic of the fundamental frequency (located at 400 nm) is found to be superimposed to a broad emission band, which is assigned to 2-photon photoluminescence. This band is observed between 400 and 650 nm. The assignment of second and third harmonic generation in Fig. 2 is based on the observed wavelengths of the sharp emission features, which corresponds to half and one-third of the wavelength of the incoming laser pulses, respectively.

The emission spectrum is recorded in two spectral regions. Third harmonic generation (see Fig. 2a) is monitored by using a laser line filter centered at 266 nm [Newport, Irvine (CA)]. Furthermore, second harmonic generation and 2-photon photoluminescence are recorded without

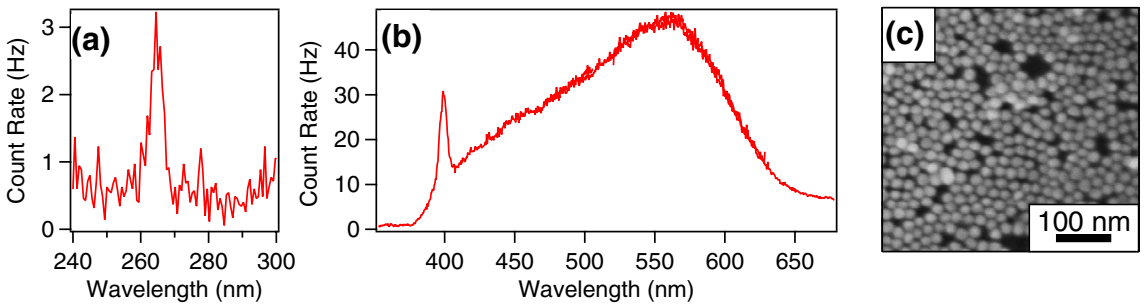

Fig. 2 Emission spectrum from ordered Au spheres ($d = 20 \pm 3$ nm) excited by femtosecond laser pulses ($\lambda = 800$ nm, peak intensity $I = 10^8$ W/cm^2, repetition rate = 80 MHz): **a** spectral region of the third harmonic of the fundamental frequency; **b** spectral region of the second harmonic of the fundamental frequency (*sharp line*) and 2-photon photoluminescence (*broad feature*); **c** electron micrograph of the nanospheres under study

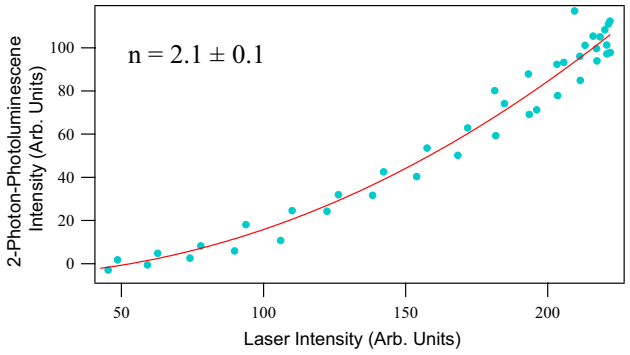

Fig. 3 Intensity dependence of photon emission from ordered Au nanoparticles ($d = 50 \pm 4$ nm) in the wavelength regime 470–650 nm, which corresponds to 2-photon photoluminescence

this filter. A second filter for suppressing the scattered 800-nm fundamental was used in both cases.

Second harmonic generation, as shown in Fig. 2b, corresponds to a surface-selective process occurring on spherical Au nanoparticles. Since the process is dipole forbidden in a sample containing inversion symmetry within the dipole approximation, it takes place only at the gold–air interface where the inversion symmetry is broken [66]. In addition, imperfections deviating from the spherical shape of the nanoparticles are known to enhance the second harmonic signal [67]. In contrast, third harmonic generation is dipole-allowed [16]. The incoherent nonlinear 2-photon photoluminescence process is known to be a useful method for the characterization of plasmonic field enhancement in metal nanostructures [68]. The broad emission feature shown in Fig. 2b is attributed to a two-step process of two sequential one-photon absorption events followed by electron–hole recombination under emission of a photon [69]. Similar findings are observed for 50 ± 4 nm, which are discussed in the following, focusing specifically on the 2-photon photoluminescence.

In Fig. 3, the intensity-dependent photon yield in the emission wavelength range between 470 and 650 nm is presented from a self-organized array prepared from 50 ± 4 nm spherical Au nanoparticles while varying the laser pulse energy using a λ/2 plate and a polarization filter. Fitting a power law to the experimental data yields $I_{\text{2-PPL}} \propto I_{\text{Laser}}^{2.1\pm0.1}$, where $I_{\text{2-PPL}}$ is the photon yield in the wavelength regime under study and I_{Laser} is the power of the exciting laser pulses. The observed quadratic relationship fully supports the assignment of 2-photon photoluminescence [70]. The magnitude of the plasmonic coupling between adjacent nanoparticles is known to depend critically on the size, shape, surface roughness, chemical composition, and interparticle distance [4, 71, 72], which indicates that it is required to adjust reliably the interparticle distance by citrate ligands, where also electrostatic repulsion is expected to play a role. The enhanced electric fields are certainly located between the particles, but also at the nanoparticle surface. Therefore, the nonlinear relationship between the 2-photon photoluminescence yield and the field intensity (see Fig. 3) makes it a well-established tool to study local field enhancement at the surface of nanostructures [73, 74].

We also investigated the laser power dependence of the third harmonics, which yields for a sample that was slightly larger than the (60 ± 5 nm) particles under study $I_{\text{THG}} \propto I_{\text{Laser}}^{2.8\pm0.3}$. The strong SHG signal from nanoparticles, as shown in Fig. 2, may appear counterintuitive at first glance. Evidently, this is due to the nanoparticle surface which provides the symmetry breaking needed for the SHG channel to be opened. In addition, any imperfections in spherical shape of the nanoparticles will enhance the SHG signal.

Figure 4 shows the spatial distribution of photon emission from nanostructured arrays of spherical Au nanoparticles ($d = 50 \pm 4$ nm) that are self-organized on a 1×1 cm^2 sapphire wafer. The diameter of the laser beam is estimated to be 100 ± 10 µm, and the mesh size for mapping the 2-photon photoluminescence response is chosen to be identical to the laser spot size.

The focal peak intensity of the laser spot is chosen to be 2×10^8 W/cm^2, which is below the damage threshold for Au nanoparticles that has been reported to be 10^{11} W/cm^2 [75]. This is consistent with our experimental results, indicating that no degradation in photon count rate is observed when returning to previously illuminated spots on the array.

Figure 4a displays regions of highly enhanced 2-photon photoluminescence emission, which is attributed to regions of the sapphire wafer where ordered Au nanostructures are found, and nanoplasmonic coupling between the nanoparticles leads to a field enhancement at the nanoparticle surface. This gives rise to nonlinear 2-photon photoluminescence (cf. Fig. 3). In order to have a robust measure of the enhancement due to plasmonic coupling, the photoluminescence intensity shown in Fig. 4a is compared to that of an aqueous dispersion of isolated Au nanoparticles of the same size. The concentration of nanoparticles in this dispersion is adjusted to 3×10^{13} particles/mL, yielding a mean interparticle distance of 261 ± 26 nm. This large interparticle distance ensures that plasmonic coupling between adjacent nanoparticles can be neglected. For the ordered nanoparticles, the interparticle distance is estimated to be 5 ± 1 nm and plasmonic coupling is expected to play a significant role for the emission of 2-photon photoluminescence. Therefore, the fluorescence signal on isolated particles defines the photon emission signal per nanoparticle that is free of collective effects. A comparison of the fluorescence count rate from isolated particles and ordered nanoparticles on a sapphire wafer yields the enhancement factor, which is attributed to nanoplasmonic coupling between neighboring nanoparticles in the nanostructure. The number of isolated

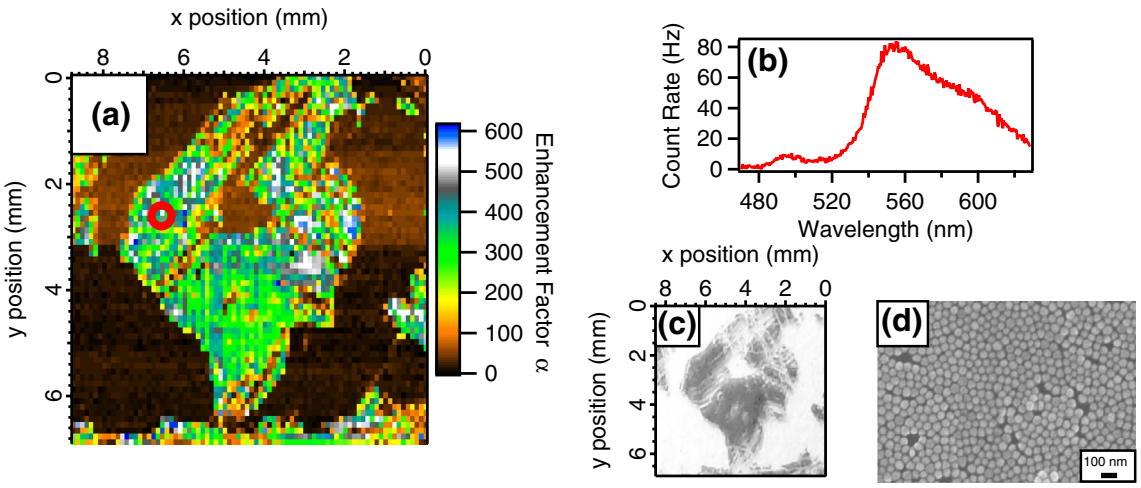

Fig. 4 Two-photon photoluminescence emitted from ordered spherical Au nanoparticles ($d = 50 \pm 4$ nm) irradiated by 800-nm laser pulses of 2×10^8 W/cm^2: **a** spatial distribution of 2-photon photoluminescence from an 8×8 mm^2 sample. The *false color scale* refers to an enhancement relative to a sample containing aqueous colloids of identical Au nanoparticles with a concentration of 3×10^{13} particles/mL, where plasmonic coupling between the nanoparticles does not occur due to large interparticle distances; **b** emission spectrum from the ordered Au nanoparticle sample shown in (**a**), where the emission is attributed to 2-photon photoluminescence recorded at the position of the *red circle* shown in (**a**); **c** photograph of the sapphire wafer. The *dark regions* correspond to areas with significant coverage of ordered nanoparticles. **d** Electron micrograph of ordered Au nanoparticles reveals predominantly a close-packed monolayer structure of gold nanoparticles. In addition, some defects are observed

nanoparticles in the laser focus in the dispersion [cuvette length: 1 mm, laser focus: 100 ± 10 µm (full width at half maximum)] is estimated to be $(2.6 \pm 0.3) \times 10^8$ particles, which contribute to the photon emission signal. The spectral shape of the photon emission from colloids and arranged nanoparticles is identical, leading to the conclusion that both contribute to 2-photon photoluminescence. In the laser focus on the substrate for a close-packed assembly of $d = 50 \pm 4$ nm Au nanoparticles and a spot size of 100 ± 10 µm, the number of excited particles contributing to the 2-photon photoluminescence signal is estimated to be 4×10^6. The enhancement factor α is then defined by the count rate per second normalized to the number of nanoparticles contained in the focal volume:

$$\alpha = \frac{I_{\text{Ordered}}}{I_{\text{Isolated}}} \tag{1}$$

Here, I_{Ordered} and I_{Isolated} refer to the 2-photon photoluminescence yield per nanoparticle in ordered arrays and from isolated nanoparticles in an aqueous dispersion, respectively.

As the yield of 2-photon photoluminescence depends quadratically on the electric near-field intensity (see Fig. 3), the enhancement factors shown in Fig. 4 correspond to the mapping of the electric near-field enhancement for each position in the nanoparticle array, where the local ordering of the nanoparticles plays a crucial role. The variation in the emission enhancement shown in Fig. 4a is understood to reflect variations in efficiency of the plasmonic coupling within the sample. Thus, regions of higher two-photon emission correspond to strong field enhancement, which is due to efficient nanoplasmonic coupling between particles. This property depends on the interparticle distance which evidently varies within the sample, as can be seen from the electron micrograph shown in Fig. 4d. There, regions of close packing of the gold nanospheres, as well as regions of less efficient packing with remarkable variety of distances on the nanometer scale are observed. Clearly, deviations from close packing are expected to result in less efficient nanoplasmonic coupling between the nanoparticles, which is due to the longer mean interparticle distance and leads in turn to a lower enhancement of the 2-photon photoluminescence. These variations in distance are far below the spatial resolution of the 2-photon photoluminescence map shown in Fig. 4a.

Figure 4a reveals an up to 600-fold enhancement of the 2-photon photoluminescence per nanoparticle in arrays, as compared to the colloidal solution samples. If the distance between the Au nanoparticles in the ordered nanostructures is sufficiently short, the near fields of individual nanoparticles overlap, which results in efficient enhancement of nonlinear optical processes. The interparticle distance is influenced on the one hand by the length of the organic ligands which determine the closest packing of the ordered nanoparticles on the substrate. An analysis of the interparticle distance in electron micrographs (see Fig. 4d) yields mean interparticle distance for close-packed Au spheres of 5 ± 1 nm along the interparticle axis. On the other hand,

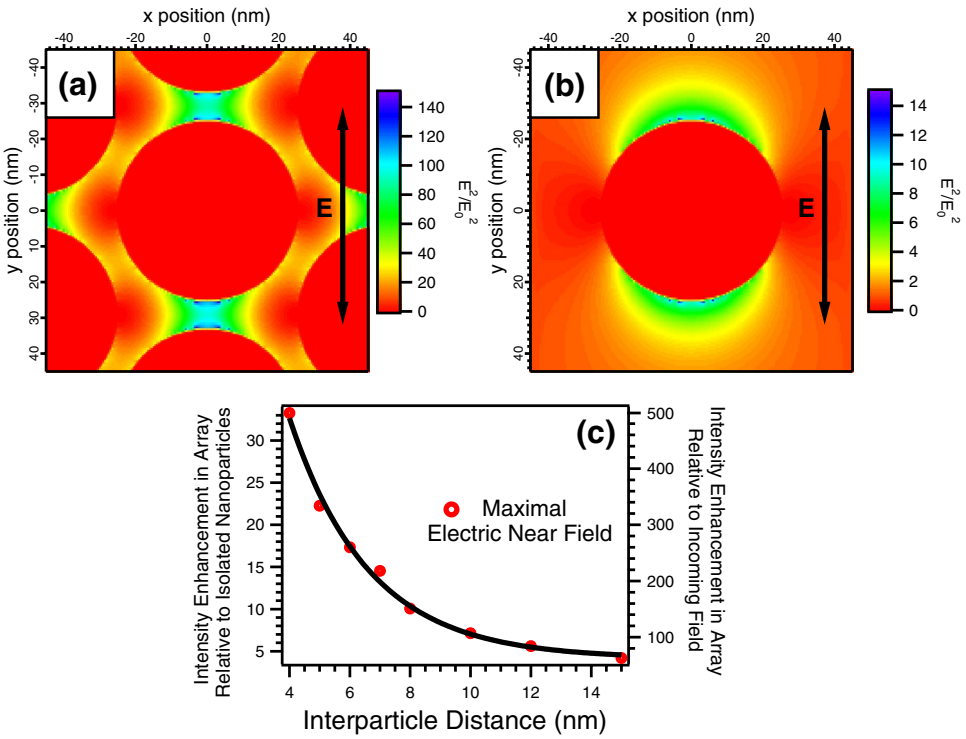

Fig. 5 Simulation of the experimental results on spherical Au nanoparticles ($d = 50$ nm, see text for further details). The incident light propagates from above the plane of the paper, and the polarization axis of the radiation is set to be vertical and is indicated by *arrows*: **a** simulation of maximal electric field amplitudes in an array with an interparticle distance of 8 nm; **b** results for a single spherical Au nanoparticle embedded in a water matrix; **c** maximum electric near-field enhancement in self-organized arrays of spherical Au nanoparticles. *Right hand axis* maximum electric near field relative to the field amplitude of the incoming laser pulses. *Left hand axis* maximum electric near field relative to isolated particles in dispersion. The *black line* serves as guide to the eye

structural defects lead to a distribution of larger distances, as can be seen in Fig. 4d, which correlates qualitatively with a lower efficiency of 2-photon photoluminescence.

A comparison of the photoluminescence map shown in Fig. 4a to a photograph of the sapphire wafer (Fig. 4c) reveals a close correlation between regions of enhanced 2-photon photoluminescence in the map (see Fig. 4a). The darker regions in the optical photograph (see Fig. 4c) are assigned as regions with significant coverage of ordered nanostructures, whereas lighter gray tones correspond to regions exhibiting less coverage due to defects. Darker regions in Fig. 4c may also be attributed to multilayers of nanoparticles, but the analysis by electron microscopy indicates that the self-organization process strongly favors monolayers of nanoparticles. These similarities support the assignment of the enhanced 2-photon photoluminescence as being due to field enhancement in the ordered nanostructures.

Finite-difference time-domain calculations are conducted in order to simulate the electric near-field enhancements by plasmonic coupling between ordered Au nanoparticles. The simulations are conducted for 50-nm particles using incident radiation with a central wavelength of 800 nm and a spectral width (full width at half maximum) of 11 nm. Thus, both the size of the nanoparticles and the laser parameters used for the simulation are similar to those used in the experiments. An array of spherical 50-nm Au nanoparticles is simulated for different distances between the close-packed spheres. The surroundings are taken to be air, and the refractive index of gold ($0.16 + 5.083i$) is taken from Ref. [76]. Furthermore, a mesh size of 0.5 nm is used for the simulations. The results of the simulation are shown in Fig. 5. For the simulations of the near-field enhancement in Au arrays, the nanoparticle surroundings are assumed to be air, rather than being dominated by the sapphire substrate. Diefenbach et al. [55] reported recently surface plasmon induced photoconductance in gold nanorods where optically induced heating of the array substrate was found to influence the plasmonic coupling between the nanoparticles. In our experiments, however, the highest field enhancements are expected between two nanoparticles, i.e., at the air–Au interface. Therefore, we do not include possible changes to the refractive index of the substrate due to heating in the present simulations.

Figure 5a shows a cut through the simulation results in the plane which contains the centers of the spheres, where the highest field enhancement is expected. The black double-headed arrow indicates the polarization axis of the laser pulses. The simulation reveals the maximum electric field enhancement to be observed when the axis connecting the nanoparticle centers is parallel to the polarization axis of the radiation. Electric near-field enhancement is also observed at the interparticle axis that has an angle of 45° to the polarization axis, but of significantly lower magnitude. For a comparison, Fig. 5b shows a similar simulation for an isolated Au nanoparticle contained in water, which corresponds to the reference system used to derive

the experimental enhancement factor. For the simulation shown in Fig. 5b, the refractive index of water ($n = 1.329$) reported by Hale and Querry [77] is used.

The results of the simulations for the maximum electric near-field enhancement in arrays of Au nanoparticles are displayed in Fig. 5c as a function of interparticle distance between the nanoparticles along the axis parallel to the polarization axis of the laser pulses. For the interparticle distances simulated, the coupling between the electron clouds of adjacent particles is significant, leading to electric near-field enhancement. The field enhancement decreases exponentially as the distance is increased, which is in agreement with previous findings [78].

The left-hand axis in Fig. 5c indicates the electric near-field enhancement in arrays compared to the near-field enhancement in identical isolated nanoparticles. The near-field intensity enhancement reaches up to 25 times the enhancement of isolated particles if the interparticle distance is around 5 nm.

Since the yield of 2-photon photoluminescence is expected to increase quadratically with the field intensity, a photon emission yield enhancement of 625 is expected, if the field enhancement factor is 25. This agrees well with the experimental findings, where an optimal emission enhancement from ordered Au spheres of 600 ± 60 times relative to that of isolated Au spheres is found for conditions in which the interparticle distance is determined to be 5 ± 1 nm. The photon emission enhancement from nanoparticles with small interparticle distances, i.e., around 4 nm, is expected to be higher, but since the focal spot is estimated to excite about 4×10^6 particles, the photon emission signal will largely reflect the most probable interparticle distance, i.e., 5 nm. Although the experimental findings indicate a maximum photon emission enhancement of 600 ± 60, several regions of lower photon emission enhancement are observed in the experimental results (see Fig. 4a). The simulations indicate that the electric near-field enhancement depends critically on the interparticle distance, and thus the experimental regions of lower photon emission enhancement are rationalizedas regions where the packing of the Au spheres deviates from close packing and may include defects, as shown in Fig. 4d. The highest field enhancements were found near nanoparticle surfaces using the FDTD method. The results depend slightly on the size of the grid that was chosen for the simulations. A choice of a smaller mesh size usually leads to higher maximal field enhancements at the nanoparticle surface. The mesh size of 0.5 nm used for the present simulations was chosen such that the experimentally observed photon emission enhancement can be reliably explained, while keeping the required computing time, which scales with the inverse third power of the mesh size, to a few hours using a personal computer. Since a smaller mesh size would result in even higher maximal field enhancements, the simulations indicate that the near-field enhancement due to plasmonic coupling is still a plausible explanation for the experimentally observed increase in photon emission.

In the context of the recent theoretical predictions of Yang et al. [60] who simulated field enhancement in arrays of 160-nm Au nanoparticles with interparticle distances of 2 nm, the interparticle distance regime explored in the present work is slightly larger. Shorter interparticle distances are expected to lead to higher electric near-field enhancements and in turn to higher photon emission yields. However, the present findings can be seen as an experimental verification of the predictions of Yang et al. [60] despite the interparticle distances in the present work being slightly larger.

4 Summary and conclusions

In conclusion, electric field enhancement in self-organized arrays of spherical Au nanoparticles (20 ± 3 and 50 ± 4 nm) due to nanoplasmonic coupling is studied. The field enhancement is quantified by measuring spatially resolved photon emission from the nanoparticle arrays, which exhibits 2-photon photoluminescence as well as second- and third harmonic generation. The photon yield of these emission channels is a sensitive probe of the efficiency of nanoplasmonic coupling between nanoparticles. An up to 600-fold increase in 2-photon photoluminescence per nanoparticle in a nanostructure is observed as compared to the yield of isolated nanoparticles in an aqueous dispersion, where the long distance between the nanoparticles rules out efficient plasmonic coupling. The results are rationalized by finite-difference time-domain simulations of arrays of self-organized Au nanoparticles. The simulations reveal a field enhancement at the surface of the nanoparticles that are arranged in an array. The field enhancement decreases exponentially with increasing distance between the nanoparticles. In the present work, the distance between the nanoparticles is 5 ± 1 nm, which reflects the choice of surface-bound ligands stabilizing the nanoparticles. There is an agreement between the present simulations and the experimental results, demonstrating that strong nanoplasmonic field enhancement explains in arrays of self-organized Au nanoparticles the 2-photon photoluminescence in arrays of nanoparticles, which cover an area of several mm^2. The present findings demonstrate an efficient, simple, and low-cost method to generate mm^2-sized arrays of ordered nanoparticles for plasmonic applications.

Acknowledgments Financial support by Deutsche Forschungsgemeinschaft (DFG) within Priority Program 1391/2 is gratefully acknowledged. M.F.K. is grateful for support by the European Union (EU) through the European Research Council (ERC) grant ATTOCO (no. 300372).

References

1. M. Kauranen, A.V. Zayats, Nonlinear plasmonics. Nat. Photonics **6**, 737–748 (2012)
2. N.J. Halas, S. Lal, W.-S. Chang, S. Link, P. Nordlander, Plasmons in strongly coupled metallic nanostructures. Chem. Rev. **111**, 3913–3961 (2011)
3. X. Wang, P. Gogol, E. Cambril, B. Palpant, Near- and far-field effects on the plasmon coupling in gold nanoparticle arrays. J. Phys. Chem. C **116**, 24741–24747 (2012)
4. P.K. Jain, M.A. El-Sayed, Plasmonic coupling in noble metal nanostructures. Chem. Phys. Lett. **487**, 153–164 (2010)
5. H. Chen, G. Wei, A. Ispas, S.G. Hickey, A. Eychmüller, Synthesis of palladium nanoparticles and their applications for surface-enhanced Raman scattering and electrocatalysis. J. Phys. Chem. C **114**, 21976–21981 (2010)
6. G.C. Schatz, Theoretical studies of surface enhanced Raman scattering. Acc. Chem. Res. **17**, 370–376 (1984)
7. E. Hao, G.C. Schatz, Electromagnetic fields around silver nanoparticles and dimers. J. Chem. Phys. **120**, 357–366 (2004)
8. S. Nie, S.R. Emory, Probing single molecules and single nanoparticles by surface-enhanced Raman scattering. Science **275**, 1102–1106 (1997)
9. S. Kühn, U. Håkansson, L. Rogobete, V. Sandoghdar, Enhancement of single-molecule fluorescence using a gold nanoparticle as an optical nanoantenna. Phys. Rev. Lett. **97**, 017402 (2006)
10. S.-Q. Zhu, T. Zhang, X.-L. Guo, X.-Y. Zhang, Self-assembly of large-scale gold nanoparticle arrays and their application in SERS. Nanoscale Res. Lett. **9**, 114 (2014)
11. H.A. Atwater, A. Polman, Plasmonics for improved photovoltaic devices. Nat. Mater. **9**, 205–213 (2010)
12. I.H. El-Sayed, X. Huang, M.A. El-Sayed, Surface plasmon resonance scattering and absorption of anti-EGFR antibody conjugated gold nanoparticles in cancer diagnostics: applications in oral cancer. Nano Lett. **5**, 829–834 (2005)
13. P. Mühlschlegel, H.-J. Eisler, O.J.F. Martin, B. Hecht, D.W. Pohl, Resonant optical antennas. Science **308**, 1607–1609 (2005)
14. A. Bouhelier, M. Beversluis, A. Hartschuh, L. Novotny, Near-field second-harmonic generation induced by local field enhancement. Phys. Rev. Lett. **90**, 013903 (2003)
15. G.F. Walsh, L. Dal, Negro, Enhanced second harmonic generation by photonic–plasmonic Fano-type coupling in nanoplasmonic arrays. Nano Lett. **13**, 3111–3117 (2013)
16. M. Lippitz, M.A. van Dijk, M. Orrit, Third-harmonic generation from single gold nanoparticles. Nano Lett. **5**, 799–802 (2005)
17. M. Sivis, M. Duwe, B. Abel, C. Ropers, Extreme-ultraviolet light generation in plasmonic nanostructures. Nat. Phys. **9**, 304–309 (2013)
18. S. Kim, J. Jin, Y.-J. Kim, I.-Y. Park, Y. Kim, S.-W. Kim, High-harmonic generation by resonant plasmon field enhancement. Nature **453**, 757–760 (2008)
19. G.F. Walsh, L. Dal, Negro, Engineering plasmon-enhanced Au light emission with planar arrays of nanoparticles. Nano Lett. **13**, 786–792 (2013)
20. F. Caruso, *Colloids and Colloid Assemblies* (Wiley-VCH, Weinheim, 2003)
21. Y.-J. Li, W.-J. Huang, S.-G. Sun, A universal approach for the self-assembly of hydrophilic nanoparticles into ordered monolayer films at a toluene/water interface. Angew. Chem. Int. Ed. **45**, 2537–2539 (2006)
22. W. Huang, W. Qian, M.A. El-Sayed, Coherent vibrational oscillation in gold prismatic monolayer periodic nanoparticle arrays. Nano Lett. **4**, 1741–1747 (2004)
23. W. Dong, H. Dong, Z. Wang, P. Zhan, Z. Yu, X. Zhao, Y. Zhu, N. Ming, Ordered array of gold nanoshells interconnected with gold nanotubes fabricated by double templating. Adv. Mater. **18**, 755–759 (2006)
24. M.A. Mangold, C. Weiss, M. Calame, A.W. Holleitner, Surface plasmon enhanced photoconductance of gold nanoparticle arrays with incorporated alkane linkers. Appl. Phys. Lett. **94**, 161104 (2009)
25. W.L. Barnes, A. Dereux, T.W. Ebbesen, Surface plasmon subwavelength optics. Nature **424**, 824–830 (2003)
26. B. Cui, L. Clime, K. Li, T. Veres, Fabrication of large area nanoprism arrays and their application for surface enhanced Raman spectroscopy. Nanotechnology **19**, 145302 (2008)
27. J. Henzie, K.L. Shuford, E.-S. Kwak, G.C. Schatz, T.W. Odom, Manipulating the optical properties of pyramidal nanoparticle arrays. J. Phys. Chem. B **110**, 14028–14031 (2006)
28. A. Sundaramurthy, P.J. Schuck, N.R. Conley, D.P. Fromm, G.S. Kino, W.E. Moerner, Toward nanometer-scale optical photolithography: utilizing the near-field of bowtie optical nanoantennas. Nano Lett. **6**, 355–360 (2006)
29. C. Aciknoz, M.A. Hempenius, J. Huskens, G.J. Vansco, Polymers in conventional and alternative lithography for the fabrication of nanostructures. Eur. Polym. J. **47**, 2033–2052 (2011)
30. N.G. Khlebtsov, L.A. Dykman, Optical properties and biomedical applications of plasmonic nanoparticles. J. Quant. Spectrosc. Radiat. Transf. **111**, 1–35 (2010)
31. Z. Nie, D. Fava, M. Rubinstein, E. Kumacheva, "Supramolecular" assembly of gold nanorods end-terminated with polymer "pom-poms": effect of pom-pom structure on the association modes. J. Am. Chem. Soc. **130**, 3683–3689 (2008)
32. T.S. Sreeprasad, A.K. Samal, T. Pradeep, One-, two-, and three-dimensional superstructures of gold nanorods induced by dimercaptosuccinic acid. Langmuir **24**, 4589–4599 (2008)
33. C. Graf, S. Dembski, A. Hofmann, E. Rühl, A general method for the controlled embedding of nanoparticles in silica colloids. Langmuir **22**, 5604–5610 (2006)
34. A. Hofmann, C. Graf, C. Boeglin, E. Rühl, Magnetic and structural investigation of Mn^{2+}-doped ZnSe semiconductor nanoparticles. ChemPhysChem **8**, 2008–2012 (2007)
35. S. Dembski, C. Graf, T. Krüger, U. Gbureck, A. Ewald, A. Bock, E. Rühl, Photoactivation of CdSe/ZnS quantum dots embedded in silica colloids. Small **4**, 1516–1526 (2008)
36. C. Graf, A. Hofmann, T. Ackermann, C. Boeglin, R. Viswanatha, X. Peng, A.F. Rodriguez, F. Nolting, E. Rühl, Magnetic and structural investigation of ZnSe semiconductor nanoparticles doped with isolated and core-concentrated Mn^{2+} ions. Adv. Funct. Mater. **19**, 2501–2510 (2009)
37. S. Perumal, A. Hofmann, N. Scholz, E. Rühl, C. Graf, Kinetics study of the binding of multivalent ligands on size-selected gold nanoparticles. Langmuir **27**, 4456–4464 (2011)
38. N.C. Bigall, A. Eychmüller, Synthesis of noble metal nanoparticles and their non-ordered superstructures. Philos. Trans. R. Soc. A **368**, 1385–1404 (2010)
39. L.M. Liz-Marzan, M. Giersig, P. Mulvaney, Synthesis of nanosized gold-silica core-shell particles. Langmuir **12**, 4329–4335 (1996)
40. C. Graf, D.L.J. Vossen, A. Imhof, A. van Blaaderen, A general method to coat colloidal particles with silica. Langmuir **19**, 6693–6700 (2003)
41. X. Lu, L. Au, J. McLellan, Z.-Y. Li, M. Marquez, Y. Xia, Fabrication of cubic nanocages and nanoframes by dealloying Au/Ag alloy nanoboxes with an aqueous etchant based on $Fe(NO_3)_3$ or NH_4OH. Nano Lett. **7**, 1764–1769 (2007)
42. R. Jin, Y. Cao, C.A. Mirkin, K.L. Kelly, G.C. Schatz, J.G. Zheng, Photoinduced conversion of silver nanospheres to nanoprisms. Science **294**, 1901–1903 (2001)

43. N.R. Jana, L. Gearheart, C.J. Murphy, Wet chemical synthesis of high aspect ratio cylindrical gold nanorods. J. Phys. Chem. B **105**, 4065–4067 (2001)
44. B. Nikoobakht, M.A. El-Sayed, Preparation and growth mechanism of gold nanorods (NRs) using seed-mediated growth method. Chem. Mater. **15**, 1957–1962 (2003)
45. G. Lee, Y.-S. Cho, S. Park, G.-R. Yi, Synthesis and assembly of anisotropic nanoparticles. Korean J. Chem. Eng. **28**, 1641–1650 (2011)
46. A. Dubavik, V. Lesnyak, N. Gaponik, A. Eychmüller, One-phase synthesis of gold nanoparticles with varied solubility. Langmuir **27**, 10224–10227 (2011)
47. C. Graf, A. van Blaaderen, Metallodielectric colloidal core-shell particles for photonic applications. Langmuir **18**, 524–534 (2002)
48. S.H. Im, Y.T. Lee, B. Wiley, Y. Xia, Large-scale synthesis of silver nanocubes: the role of HCl in promoting cube perfection and monodispersity. Angew. Chem. Int. Ed. **44**, 2154–2157 (2005)
49. J. Ren, R.D. Tilley, Preparation, self-assembly, and mechanistic study of highly monodispersed nanocubes. J. Am. Chem. Soc. **129**, 3287–3291 (2007)
50. L.J. Sherry, R. Jin, C.A. Mirkin, G.C. Schatz, R.P. Van Duyne, Localized surface plasmon resonance spectroscopy of single silver triangular nanoprisms. Nano Lett. **6**, 2060–2065 (2006)
51. S. Roorda, T. van Dillen, A. Polman, C. Graf, A. van Blaaderen, B.J. Kooi, Aligned gold nanorods in silica made by ion irradiation of core-shell colloidal particles. Adv. Mater. **16**, 235–237 (2004)
52. J. Liao, L. Bernard, M. Langer, C. Schönenberger, M. Calame, Reversible formation of molecular junctions in 2D nanoparticle arrays. Adv. Mater. **18**, 2444–2447 (2006)
53. J. Liao, S. Blok, S.J. van der Molen, S. Diefenbach, A.W. Holleitner, C. Schönenberger, A. Vladyka, M. Calame, Ordered nanoparticle arrays interconnected by molecular linkers: electronic and optoelectronic properties. Chem. Soc. Rev. **44**, 999–1014 (2015)
54. T.K. Sau, C.J. Murphy, Self-assembly patterns formed upon solvent evaporation of aqueous cetyltrimethylammonium bromide-coated gold nanoparticles of various shapes. Langmuir **21**, 2923–2929 (2005)
55. S. Diefenbach, N. Erhard, J. Schopka, A. Martin, C. Karnetzky, D. Iacopino, A.W. Holleitner, Polarization dependent, surface plasmon induced photoconductance in gold nanorod arrays. Phys. Status solidi (RRL) **8**, 264–268 (2014)
56. R. Kodiyath, S.T. Malak, Z.A. Combs, T. König, M.A. Mahmoud, M.A. El-Sayed, V.V. Tsukruk, Assemblies of silver nanocubes for highly sensitive SERS chemical vapor detection. J. Mat. Chem. A **1**, 2777–2788 (2013)
57. F. Le, D.W. Brandl, Y.A. Urzhumov, H. Wang, J. Kundu, N.J. Halas, J. Aizpurua, P. Nordlander, Metallic nanoparticle arrays: a common substrate for both surface-enhanced Raman scattering and surface-enhanced infrared absorption. ACS Nano **2**, 707–718 (2008)
58. M.B. Raschke, High-harmonic generation with plasmonics: feasible or unphysical? Ann. Phys. **525**, A40–A42 (2013)
59. M. Sivis, M. Duwe, B. Abel, C. Ropers, Nanostructure-enhanced atomic line emission. Nature **485**, E1–E2 (2012)
60. Y.-Y. Yang, A. Scrinzi, A. Husakou, Q.-G. Li, S.L. Stebbings, F. Süßmann, H.-J. Yu, S. Kim, E. Rühl, J. Herrmann, X.-C. Lin, M.F. Kling, High-harmonic and single attosecond pulse generation using plasmonic field enhancement in ordered arrays of gold nanoparticles with chirped laser pulses. Opt. Express **21**, 2195–2205 (2013)
61. J. Plenge, A. Wirsing, I. Wagner-Drebenstedt, I. Halfpap, B. Kieling, B. Wassermann, E. Rühl, Coherent control of the ultrafast dissociative ionization dynamics of bromochloroalkanes. Phys. Chem. Chem. Phys. **13**, 8705–8714 (2011)
62. E. Antonsson, C. Peltz, J. Plenge, B. Langer, T. Fennel, E. Rühl, Signatures of transient resonance heating in photoemission from free NaCl nanoparticles in intense femtosecond laser pulses. J. Electron Spectrosc. Relat. Phenom. **200**, 216–221 (2015)
63. E.Y. Hleb, D.O. Lapotko, Photothermal properties of gold nanoparticles under exposure to high optical energies. Nanotechnology **19**, 355702 (2008)
64. J. Turkevich, P.C. Stevenson, J. Hillier, A study of the nucleation and growth processes in the synthesis of colloidal gold. Discuss. Faraday Soc. **11**, 55–75 (1951)
65. K.S. Yee, Numerical solution of initial boundary value problems involving Maxwell's equations in isotropic media. IEEE Trans. Antennas Propag. **14**, 302–307 (1966)
66. Y.R. Chen, Optical second harmonic generation at interfaces. Annu. Rev. Phys. Chem. **40**, 327–350 (1989)
67. J. Nappa, G. Revillod, I. Russier-Antoine, E. Benichou, C. Jonin, P. F. Brevet, Electric dipole origin of the second harmonic generation of small metallic particles. Phys. Rev. B **71**(16), 165407 (2005)
68. K. Ueno, H. Misawa, Fabrication of nanoengineered metallic structures and their application to nonlinear photochemical reactions. Bull. Chem. Soc. Jpn **85**, 843–853 (2012)
69. K. Imura, T. Nagahara, H. Okamoto, Near-field two-photon-induced photoluminescence from single gold nanorods and imaging of plasmon modes. J. Phys. Chem. B **109**, 13214–13220 (2005)
70. A. Bouhelier, R. Bachelot, G. Lerondel, S. Kostcheev, P. Royer, G.P. Wiederrecht, Surface plasmon characteristics of tunable photoluminescence in single gold nanorods. Phys. Rev. Lett. **95**, 267405 (2005)
71. T. Götz, M. Buck, C. Dressler, F. Eisert, F. Träger, Optical second-harmonic generation by supported metal clusters: size and shape effects. Appl. Phys. A **60**, 607–612 (1995)
72. M.I. Stockman, D.J. Bergman, C. Anceau, S. Brasselet, J. Zyss, Enhanced second-harmonic generation by metal surfaces with nanoscale roughness: nanoscale dephasing, depolarization, and correlations. Phys. Rev. Lett. **92**, 057402 (2004)
73. M.R. Beversluis, A. Bouhelier, L. Novotny, Continuum generation from single gold nanostructures through near-field mediated intraband transitions. Phys. Rev. B **68**, 115433 (2003)
74. J. Beermann, T. Sondergaard, S.M. Novikov, S.I. Bozhevolnyi, E. Devaux, T.W. Ebbesen, Field enhancement and extraordinary optical transmission by tapered periodic slits in gold films. New J. Phys. **13**, 063029 (2011)
75. J. Güdde, J. Hohlfeld, J.G. Müller, E. Matthias, Damage threshold dependence on electron–phonon coupling in Au and Ni films. Appl. Surf. Sci. **127–129**, 40–45 (1998)
76. P.B. Johnson, R.W. Christy, Optical constants of the noble metals. Phys. Rev. B **6**, 4370–4379 (1972)
77. G.M. Hale, M.R. Querry, Optical constants of water in the 200-nm to 200-μm wavelength region. Appl. Opt. **12**, 555–563 (1973)
78. O. Lecarme, T. Pinedo-Rivera, K. Berton, J. Berthier, D. Peyrade, Plasmonic coupling in nondipolar gold colloidal dimers. Appl. Phys. Lett. **98**, 083122 (2011)